Conference paper

Petr Viščor* and Martin Viščor

Electrical Impedance Spectroscopy: "First Principles" analysis and simulations of electrical response in the classical range of frequencies below 1 THz and the resulting new role of Electrical Impedance Spectroscopy in electrical characterisation within Condensed Matter Physics

https://doi.org/10.1515/pac-2018-1107

Abstract: In order to investigate the full potential of the Electrical Impedance Spectroscopy (EIS) when used to address various aspects of conductive and dielectric response within the field of Condensed Matter Physics and Electrochemistry, a new analysis of the electrical impedance experiments has been undertaken. Within the framework of quantum mechanical band structure and using the concept of electrochemical potential for each of the relevant energies, the problem of electrical response in condensed phase has been formulated, using augmented Maxwell equations of Classical Electrodynamics, as a boundary value problem of a set of coupled, non-linear parabolic equations in energy, space and time. The result of this numerical analysis is a principal possibility of a complete electrical characterisation of both monocrystals, glassy solids and liquids. The EIS has been put in this way on a new qualitative level and should be considered now as the most general electrical experimental characterisation tool available. In this article, a methodology of numerical simulations of electrical response in condensed matter systems at classical frequencies (from ~1 THz down to dc) is presented and the numerical simulation results are then discussed, using monocrystalline Silicon, chalcogenide glass ion conductor $Ag_x(AsS_2)_{1-x}$ and simple aqueous chloride solution as experimental test cases. Some other unique results of the new EIS analysis will also be discussed. These include the possibility of a clear distinction between the contribution to the electrical response from bound and mobile electrical charges, the possibility of simultaneous and independent determination of the mobile electrical charges mobility and their density in one EIS experiment and incorporation of the interfacial regions of the system under test (SUT) as an essential part of the overall electrical response.

Keywords: Condensed Matter Physics; dielectric relaxation; electrical characterisation methods; electrical response; electrical transport; electrochemistry; insulators; physics of glasses; semiconductor physics; SSC-2018.

Introduction

The EIS has been used, in a variety of forms, to study electrical resistive, capacitive and inductive physical processes in materials ever since mid-18th century [1]. The EIS experiment itself (measurement of electrical current in response to externally applied voltage, both varying harmonically in time) has evolved

Article note: A collection of invited papers based on presentations at the 13th International Conference on Solid State Chemistry (SSC-2018), Pardubice, Czech Republic, September 16–21, 2018.

***Corresponding author: Petr Viščor,** EIS Laboratory, Skjoldenaesvej 17, 4174 Jystrup, Denmark; Institute of Applied Physics and Mathematics, University of Pardubice, Pardubice, Czech Republic; Joint Glass Center, Alexander Dubcek University of Trencin, Trencin, Slovak Republic; and Semimetrics Ltd., Kings Langley, England, e-mail: viscorpetr@gmail.com
Martin Viščor: CEZ, Duhova 1, Prague, Czech Republic; and National University of Ireland, Cork, Republic of Ireland

considerably since then, and today there are available commercial, high precision instruments covering the entire frequency range of interest (from dc to ~1 THz). The data obtained are usually very rich in structure and information and it is therefore surprising that even today, the analysis is often still on the level of *quasi*-analytic approximations [1–3] and various *Equivalent R, C, L model networks*. The analysis and modelling of the measured response using equivalent R, C, L model networks is almost always phenomenological and often arbitrary. Such R, C, L models of the measured electrical response very often lack deeper physical meaning that should connect them in a direct way to the actual physical microscopic processes which they are supposed to model.

This and some un-answered and quite fundamental questions in the physics of non-crystalline materials [4–6] in particular, has led the present authors to take a new approach to the study and analysis of electrical response in condensed phase below Tera Hertz frequencies and its relation to the Electrical Impedance measurements. In this new approach, the electrical response of a piece of material to externally applied electrical field is sought in terms of space-time evolution of the total, local electrical charge density $\rho(x, t)$, by solving Maxwell equations of Classical Electrodynamics with appropriate boundary conditions. The material is for the purpose of the analysis characterised by a set of relevant quantum mechanical energy levels (simplified electron energy band structure). The occupation of these energy levels by electrical charges (electrons, holes, polarons and/or ions, etc.) is governed by appropriate statistics (Fermi-Dirac or Boltzmann) and the particle fluxes are determined by the gradients of the respective *quasi*-electrochemical potentials. The result of the analysis is then the space-time dependent total, local electrical charge density $\rho(x, t)$ that is directly related to experimentally measurable complex electrical admittance of SUT.

With a Heaviside voltage step input for example, the space-time evolution of $\rho(x, t)$ and the corresponding total, local electrical current density $i(x, t)$ determine the real time electrical admittance $Y(t)$ of SUT. This quantity, through Laplace transform, is then directly related to the experimentally observable complex, and in general frequency dependent, electrical admittance $\tilde{Y}(\omega)$ of the material.

The results of the new numerical analysis and simulations of the electrical response and of the electrical impedance experiment have turned out to be quite far reaching.

On one side, it is the EIS experiment itself [1–3]. The new EIS numerical analysis enables determination of a large number of electrical material parameters in the SUT, inclusive simultaneous determination of electrical mobility and density of mobile electrical charges. This could have been achieved previously only by using a large number of other experimental methods. In this way, the new analysis has put EIS on a completely new qualitative level as an electrical characterisation tool. It could be argued now that instead of being just …*one of possible electrical characterisation methods*…, it has become … *the most important electrical characterisation method*…, whereby the other methods are either a single point on or some parts of the complex electrical impedance $\tilde{Z}(\omega)$ curves, measured by EIS.

On the other side, it is the modelling and simulation of the electrical response in various substances. The new EIS analysis shows that EIS is the most general and direct experimental manifestation of the various solutions of Maxwell equations of Classical Electrodynamics, describing electrical response in various materials under various conditions. This allows numerical simulation and testing of various models of electrical response in condensed phase.

The aim of this paper is to present the new EIS analysis in a clear and simple manner, without going to un-necessary details both in EIS experiment and in the EIS analysis itself. To that effect and wherever possible, the reference will be made to other relevant monographs and articles on the subject at hand.

The present paper is structured as follows. The methodology of the new EIS analysis will be presented in Section 2. The main ingredients of the analysis and the structure of the governing equations will be shortly discussed and their numerical solutions outlined. The connection between the numerical solution and experimentally obtainable complex electrical impedance $\tilde{Z}(\omega)$ of the SUT will also be explained.

The results of the new EIS numerical analysis will be demonstrated on EIS experiments using monocrystalline Silicon, chalcogenide glass ion conductor and simple aqueous chloride liquid solution in Section 3. A short summary of all electrical material parameters that can be determined in a single EIS experiment

will also be given. Important in the context of the obtained numerical results is the connection between the full numerical results leading to the experimentally observable model electrical impedance and the possible equivalent R, C, L network of the same. It will be shown that this connection is quite unique. The numerical solutions determine not only the topology of such R, C, L networks, but also the analytical values of the various R, C, L elements in terms of the SUT electrical material parameters [2]. This result is considered quite important and puts also R, C, L networks modelling on a new qualitative level. Finally, including SUT boundaries as an essential element of the EIS numerical analysis, leads to a quite unique possibility to determine free electrical charge mobility and their density independently in a single EIS experiment. This important aspect of the new EIS numerical analysis will also be demonstrated and discussed, using EIS data and the new EIS analysis on both monocrystalline Silicon, but also on chalcogenide glass ion conductor ($Ag_x(AsS_2)_{1-x}$). The relation between the new EIS method and other electrical characterisation methods will be taken up next. Both the real time methods and frequency domain methods will be shortly discussed to illustrate the general strength of new EIS methodology.

The main results and conclusions will be summarised in Section 4.

Methodology – new EIS numerical analysis posed as a non-linear, parabolic boundary value problem

The main goal of the new EIS numerical analysis has been to describe the energy-space-time evolution of all electrical charges and the respective space-time dependent currents in the SUT and to relate these to the experimentally measurable electrical impedance $\tilde{Z}(\omega)$ of the SUT. In order to achieve this goal, the theoretical framework of the analysis contains some necessary elements of quantum mechanics, thermodynamics and Classical Electrodynamics.

The space-time scales considered are *macroscopic* in the spirit of Landau [7, 8] and are of the order of time $\geq 10^{-12}$ s (1 ps) and space $\geq 1.0 \cdot 10^{-7}$ cm (10 Å). Following Landau, this means, that the times considered are *classical* and are larger than a characteristic microscopic time in the SUT (a typical Debye phonon frequency). The space considered is such that the microscopic variations of atomic potentials are "averaged out". Maxwell equations used are therefore *macroscopic* [8] and the minimum, mesoscopic space volume considered is such that the local thermodynamic equilibrium is still well defined with thermodynamic quantities such as temperature, pressure, chemical potential etc. Thermodynamic non-equilibrium characteristics such as currents and transport coefficients are then obtained in near equilibrium limit.

The presented analysis is One-Dimensional (1D) because the samples are assumed to be homogeneous in y–z plane and the necessary condition for the 1D treatment is also satisfied ($\sqrt{\text{Area}} \gg \text{Thickness}$). In other words, the samples are assumed to be thin platelets of Area $= A_S$ and the Thickness $= L_S$.

All electrically charged particles are placed onto their respective, relevant energy levels E_j (quantum mechanical or classical) and the densities of these electrical charges at these levels are governed by Fermi-Dirac or Boltzmann statistics, using the respective *quasi*-electrochemical potentials [9]. In order to keep the presentation of the new EIS analysis as simple as possible, only electrons, and this includes therefore also holes, are considered. The analysis is though equally valid for the case of classical particles such as various ions, electrically active (charged) molecules and other more macroscopic and charged molecular aggregates. The effect of electrode-sample interfaces are incorporated into the analysis via the respective electrode and sample chemical potentials. One considers here real samples that are finite (existence of real surfaces) and are connected to the external voltage source and measuring circuit via well-defined electrodes.

The new EIS analysis will be presented in three stages: The sample definition and the calculation of thermal equilibrium, the calculation of the steady state under the influence of external dc voltage bias perturbation and finally the calculation of the detailed time response of the SUT to a small, measuring voltage perturbation.

Sample definition and the thermodynamic equilibrium

Starting with sample definition, Fig. 1 shows the simplified electron energy band diagram for a typical sample (semiconductor in this case) before any contact between the sample and the electrodes have been made. The *x* co-ordinate in this and in the most of the following figures is non-linear. The x-cells have different thicknesses in order to capture clearly the spatial variations of various variables within both the bulk and the thin interface regions.

Here, the blue line represents the bottom of the conduction band E_c, having effective density of states N_c and being occupied by free electrons with density n_e. Likewise, the red line represents the top of the valence band E_v, having effective density of states N_v and being occupied by free holes with density n_h. The black dash-dot line represents a deep, strongly localised defect energy level E_j, placed within the forbidden energy gap of this model semiconductor, having the density N_j. It is occupied by electrons with density n_j, which are strongly localised when occupying this level. Finally, the magenta dashed line represents the electron chemical potential in the bulk of the sample and the electron chemical potential at the metal electrode-sample interface. The model sample is of finite thickness L_S and area A_S, with left and right interfaces also indicated in Fig. 1. Under the condition of the electrical charge neutrality deep within the bulk, the respective *quasi*-chemical potentials [9], defined at each relevant energy level, collapse to a single level, the bulk chemical potential *chpotB*. Before the electrical contact to the electrodes is established, the chemical potential of the sample *chpotB* is at different energy relative to the energy of the left and right electrodes chemical potentials *chpotSl* and *chpotSr*. In order to simplify terminology, the term *electrochemical potential* will be used throughout this article from now on, even in the absence of any internal electrical fields and potentials [9]. It is also important to mention here that in solid state physics, the term *Fermi energy/level* is often used instead of *chemical/electrochemical potential*.

When the electrical contact is made to the external electrodes, the difference between the sample bulk electron chemical potential *chpotB* and the respective electron chemical potentials of the left and the right electrodes *chpotSl* and *chpotSr* will cause electron flow across the interfaces and mobile charge depleted or mobile charge accumulated regions near the electrode-sample interfaces will be formed. The changing non-zero local, total electrical charge density $\rho(x, t)$ and the correspondingly changing internal electrical field and potential will lead eventually to the state of thermodynamic equilibrium, where the SUT electrochemical *elchpotB* potential is constant across the entire system left electrode-sample-right electrode. Also now, the respective *quasi*-electrochemical potentials collapse to this single level. The situation of this thermodynamic

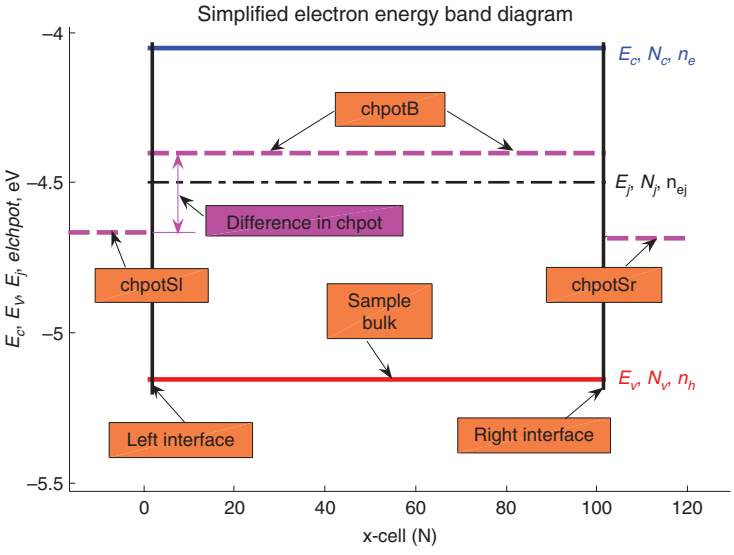

Fig. 1: Simplified electron energy band diagram of a model semiconductor sample with interfaces before contact is made.

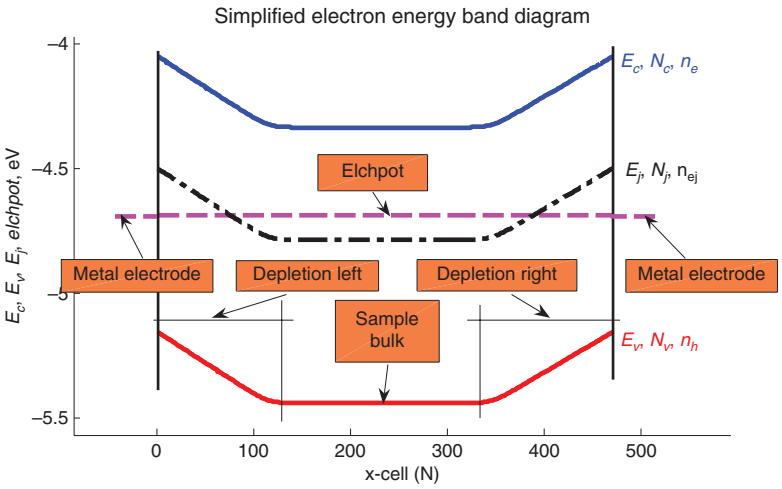

Fig. 2: Simplified electron energy band diagram of a model semiconductor sample with interfaces after contact is made.

equilibrium for a positive *difference in chpot* in Fig. 1, when electrons flow from the interior of the sample into electrodes, is shown in Fig. 2.

The resulting thermo-equilibrium $\rho(x, t\to\infty)$ is found as the solution of Poisson equation, relating the electrical charge density to the corresponding electrical potential. The result is that *elchpot* in Fig. 2 is a constant, independent of space variable x.

External perturbation and the steady state

When an external, electrical perturbation, such as voltage step for example, is applied across the system, shown in Fig. 2, finite electrical currents will be induced within the sample. These particle fluxes and corresponding electrical currents are governed by the gradients of the respective *quasi*-electrochemical potentials:

$$j(n_j, E_j, x, t) = -\frac{n_j(E_j, x, t)\cdot\mu(E_j, x, t)}{|e|}\cdot grad[elchpot(E_j, x, t)] \tag{1}$$

Here, $j(n_j, E_j, x, t)$ is the particle flux density [1/M$^2\cdot$s], $n_j(E_j, x, t)$ is the density of the mobile charge particles of the type j (electron, hole, polaron, ion, etc.) at energy E_j, at space co-ordinate x and at time t, $|e|$ is the absolute value of the elementary charge and $elchpot(E_j, x, t)$ is the *quasi*-electrochemical potential for electrons (particles) at energy level E_j, co-ordinate x and time t. It should be mentioned here that the units in the present article are SI units, unless explicitly specified. An exception is energy, which is given in electron-Volts [eV]. Already at this stage it is clear that the concept of the electrochemical potential plays quite important role in the present analysis. Here it is calculated directly from the Fermi-Dirac statistical function

$$elchpot(E_j, n_j, x, t) = E_{j0} - |e|\cdot V(x, t) - kT\cdot\ln\left[\left(\frac{N_j}{n_j(E_j, x, t)} - 1\right)\cdot\frac{1}{g(E_j)}\right], \tag{2}$$

where $elchpot(E_j, n_j, x, t)$ is the *quasi*-electrochemical potential for particles n_j at energy E_j and E_{j0} is the position of E_j at zero electrical potential, usually taken to be zero at the left interface, where the x co-ordinate is taken to be equal zero. $V(x, t)$ is the electrical potential within the sample, k is Boltzmann constant, T is the absolute temperature and $g(E_j)$ is the degeneracy factor for energy E_j. This *short cut*, avoiding the complexities

of the thermodynamic calculation is felt well justified in the light of *sample definition*, shown in Fig. 2, when the sample is defined at constant temperature and pressure, with known (modelled) spectrum of energies and corresponding particle densities.

The external voltage applied to the sample, chosen in the present analysis, is the Heaviside voltage step. Although this choice has been made mainly for computational reasons and does not limit in any sense the generality of the analysis, it has an advantage which will become clear later when discussing mobile charge polarisation effects. It is also felt that the discussion of various aspects of the electrical response is easier and more illustrative when this type of input is used rather than the sinusoidal input.

Once the sample, the thermodynamic equilibrium (solution of Poisson equation) and the local space-time dependent currents [eq. 1] are defined, the steady state response to a given step voltage input can be calculated. The dynamics of the space-time evolution of electrical charge density $\rho\ (x, t)$ and of local, electrical currents' densities $i(n_j, E_j, x, t) = \pm |e| \cdot j(n_j, E_j, x, t)$ towards this steady state is governed by Maxwell equations of Classical Electrodynamics [8, 10]:

$$\mathrm{div}\ \vec{E} = \frac{\rho}{\varepsilon_0} \tag{3}$$

$$\mathrm{rot}\ \vec{E} = -\frac{\partial \vec{B}}{\partial t} \tag{4}$$

$$\mathrm{div}\ \vec{B} = 0 \tag{5}$$

$$\mathrm{rot}\ \vec{H} = i + \frac{\partial \vec{D}}{\partial t} \tag{6}$$

Here, $\vec{E}$ is the electrical field intensity, ρ is the total, local electrical charge density $\rho(x, t)$, ε_0 is the dielectric permittivity of vacuum, $\vec{B}$ is the magnetic field induction, i is the electrical current density due to free, mobile charges and $\vec{D}$ is the electric field induction [10]. The relation of $\vec{D}$ and $\vec{B}$ to fields $\vec{E}$ and $\vec{H}$ and to media electromagnetic properties is given by

$$\vec{D} = \varepsilon_0 \cdot \vec{E} + \vec{P} = \varepsilon \cdot \vec{E} \tag{7}$$

$$\vec{B} = \mu_{\mathrm{mag0}}(\vec{H} + \vec{M}) = \mu_{\mathrm{mag}} \cdot \vec{H} \tag{8}$$

Here, ε_0 is the dielectric permittivity of vacuum, $\vec{P}$ is the media polarisation, ε is the dielectric permittivity of the media, $\vec{H}$ is the magnetic field intensity, μ_{mag0} is the magnetic permeability of vacuum, $\vec{M}$ is the media magnetisation and μ_{mag} is the media magnetic permeability. Media/material electromagnetic properties are then given by the dielectric permittivity ε, by the magnetic permeability μ_{mag}, by free electrical charge mobility $\mu(E_j, x, t)$ and the corresponding mobile charge density $n_j(E_j, x, t)$ [eq. 1].

Once the boundary conditions are defined, the eqs. 1 to 8 form a complete set to be solved for $\rho(x, t)$. Forced by the finite speed of today computers and by the complexity of the problem at hand, a number of simplifying assumptions/approximations though have had to be made:

Assumption 1. The electrical charges discussed here are considered to be independent *quasi*-particles [7]. Their mutual interaction is *hidden* in the electrochemical potential and in the electrical fields they create [eq. 3].

Assumption 2. The total, local electrical charge density $\rho(x, t)$ can be written as sum of free and bound electrical charges

$$\rho(x,t) = \rho(x,t)_{\mathrm{Free}} + \rho(x,t)_{\mathrm{Bound}} \tag{9}$$

The free electrical charges at various energies have non-zero electrical mobilities $\mu(E_j, x, t)$ and contribute to the electrical current density i in eq. 6, while the bound charges, with their electrical mobilities at a given energy being zero, contribute to the electrical induction $\vec{D}$ in eq. 6.

A further comment, relating the Equations (6) and (9) to time dependent electrical measurements, such as EIS, might be appropriate at this stage. Both quantities on the right hand side of Eq. (6) are electrical current densities. While the first term, due to mobile electrical charges, is directly proportional to the electrical field intensity $\vec{E}$ (resistive response), the second term, due to bound charges, is proportional to the time derivative of this field. For sin/cos input voltage, this means a 90 degrees shift between the applied input voltage and measured output current (capacitive response). This difference is captured, at least in principle, by EIS method.

Assumption 3. The two fundamental electrical material parameters of the investigated medium are electrical mobility $\mu(E_j, x, t)$ and the dielectric permittivity (dielectric response function) $\varepsilon(x, t)$. In the present new EIS analysis, they are assumed to be time independent. Their possible spatial dependence though is taken into account. Later, it will be argued that for times longer than 1 ps [7], the mobility of electrical charges is indeed constant $\mu(E_j, x)$, irrespective of whether these charges move in the extended energy states with finite scattering rates or in the localised states with finite hopping rates. The situation is less satisfactory in regards dielectric permittivity becoming time independent dielectric constant $\varepsilon(x)$. With this assumption, it would appear that the slow polarisation processes with relaxation times longer than some 1 ps cannot be captured by the present analysis. This is not completely true. It will be shown later that the new EIS analysis leads to a possibility to model the electrical response quite precisely also in terms of approximate R, C, L networks. However, and contrary to present days R, C, L modelling, these networks have unique topology and the values of various R, C, L elements are analytic functions of the medium electrical material parameters. Using generalised R, C elements, it is therefore possible to analyse even the slow polarisation processes. The simplifying assumption concerning the dielectric permittivity has been dictated by the general complexity of the numerical analysis when the dispersion of the medium is to be taken into account [10]. For the purpose of clarity and simplicity, the dielectric permittivity $\varepsilon(x, t)$ will be from now on called in short just the dielectric permittivity also when it is just a space-time independent constant (dielectric constant).

Assumption 4. Magnetic field effects are neglected which means that the present new EIS analysis is centred around electrical rather than electromagnetic response and some of the electromagnetic wave-like phenomena might be lost. It is argued that this is not too a severe approximation in view of space-time scales considered here.

Assumption 5. Within the framework of the present analysis, when the electrical charges move at various energy levels and can be transferred among them through finite transition rates, the concept of charge conservation for charges at these energy levels is not really valid and the Maxwell eq. 6 has to be augmented by the appropriate sinks and sources.

With the assumptions (1)–(5) in mind, the set of equations that governs space-time evolution of the total, local electrical charge density $\rho(x, t)$ can be summarised as follows:

$$\operatorname{div} \vec{E} = \frac{\rho(x,t)}{\varepsilon_0} \tag{10}$$

$$\operatorname{rot} \vec{E} = 0 \tag{11}$$

$\operatorname{div} \cdot \operatorname{rot} \vec{H} = 0 = \operatorname{div}(i) + \operatorname{div}\left(\frac{\partial \vec{D}}{\partial t}\right)$, which becomes, after some manipulation and adding sinks and sources

$$\frac{\partial \rho(E_j, x, t)}{\partial t} = -\operatorname{div}[i_j(E_j, x, t)] + \text{sources}_j - \text{sinks}_j \quad \text{(one equation for each energy } E_j\text{)} \tag{12}$$

$$\vec{D} = \varepsilon \cdot \vec{E} \tag{13}$$

$$i(n_j, E_j, x, t) = \mp|e| \cdot j(n_j, E_j, x, t) = + \frac{n_j(E_j, x, t) \cdot \mu(E_j, x, t)}{1} \cdot grad[elchpot(E_j, x, t)] \tag{14}$$

$$elchpot(E_j, n_j, x, t) = E_{j0} - |e| \cdot V(x, t) - kT \cdot \ln\left[\left(\frac{N_j}{n_j(E_j, x, t)} - 1\right) \cdot \frac{1}{g(E_j)}\right] \tag{15}$$

Boundary conditions are, for the purpose of this article, of Dirichlet type, fixing the electrical charge density at the boundaries through electrochemical potentials of the respective electrodes.

The eqs. 10–15 form a set of coupled, non-linear equations of parabolic type that is very boundary conditions sensitive. As already mentioned, the mobile electrical charges here are considered free, interacting with each other only through the internal electrical field they generate. The numerical solution, the details of which will be described in another article of these series, gives the space-time evolution of the total, local electrical charge density $\rho(x, t)$ and the local electrical current densities $i(n_j, E_j, x, t)$. The space integrals of these currents (one for each relevant energy level) at each time interval, multiplied by the effective area of the electrodes A_S then give the wanted total electrical current $I(t)$, flowing through the system in response to the applied voltage step $V(t)$. A typical time dependence of $I(t)$ for a given model semiconductor (ultra pure monocrystalline Silicon with a very small, residual density of a single deep level defect) is shown in Fig. 3.

When the steady state is reached, the total, local current density $i(x, t)$ becomes space and time independent, with the resulting total electrical current through the system $I(t)$ reaching a final, time independent constant value. In Fig. 3, this happens for times longer than ~0.01 s. The respective, *quasi*-electrochemical potentials $elchpot(E_j, n_j, x, t)$ at the reached steady state are now space dependent functions, in principle different for each different energy level E_j. In the above given example, one can already now see various aspects of a general electrical response in a system consisting of a given sample and the electrodes – SUT. Some of these aspects might be worthwhile pointing out:

- The current $I(t)$ relaxation towards steady state is non-exponential.
- The time dependence of $I(t)$ is not caused by time/frequency dependent electrical mobility $\mu(E_j, x, t)$ or time/frequency dependent dielectric permittivity $\varepsilon(x, t)$. Both parameters are energy and space/time independent constants.
- The relaxation of the system without deep level defect (green curve in Fig. 3) towards steady state is not caused by some slow polarisation of bound charges, but it is solely due to the movement of the electrical mobile charges in the system. This type of polarisation is termed here and from now on

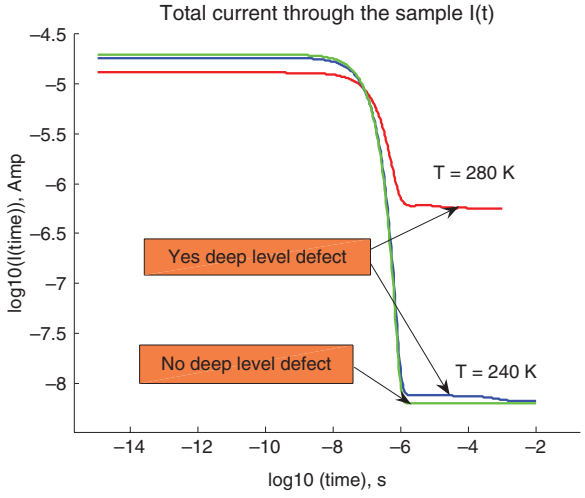

Fig. 3: Total electrical current $I(t)$ through the model semiconductor sample as a function of time, after application of a Heaviside step voltage at time t = 0.

as *mobile charge polarisation*. The bound charges polarisation (dielectric permittivity ε) affects only the value of the characteristic relaxation time $\tau_{relax} = \frac{\varepsilon}{\sigma}$, where σ is the dc conductivity of the medium ($\sigma = |e| \cdot n \cdot \mu$). The τ_{relax} is around $3 \cdot 10^{-7}$ s in Fig. 3.

– The relaxation due to deep level defect (blue curve in Fig. 3, in the time range 10^{-6} to 10^{-2} s) is non-Debye like and falls into the class of *Universal Relaxation* [11–13].

Time response of the system and the complex frequency dependent admittance

The ratio $I(t)/V(t)$ defines the real time admittance $Y(t)$ of the system. When the input step voltage is sufficiently small (requirement of the linear response), $Y(t)$ can be related directly, via Laplace transform, to the measurable, frequency dependent admittance of the system $\tilde{Y}(\omega)$, where the frequency ω is related to the measurement frequency f [Hz] through $\omega = 2\pi \cdot f$. The corresponding final result of the analysis for the model semiconductor shown in Fig. 3, is presented in Fig. 4.

Here and in all the following figures, the raw EIS experimental data are shown as red dots, while the calculated EIS response are the continuous green curves, unless stated otherwise. Two plateaus can be identified in the real part of $\tilde{Y}(\omega)$, shown in Fig. 4. The high frequency plateau is the dc admittance of the bulk of the model semiconductor sample, while the low frequency plateau is the dc admittance of the high resistive electrode-sample interface, marked as Depletion in Fig. 4. In the transition region between these two levels, the real part of the admittance varies approximately as $Y_1(\omega) \sim \omega^{1.9}$.

The electrical response, shown in Fig. 4, is quite general and it is characteristic of any material consisting of sample bulk and electrodes-sample bulk interfaces. This observation applies also to non-crystalline materials, liquids and other disordered systems. Here though, often only one plateau is measured and the observed slope is often of the *universal relaxation* type [11–13] with $Y_1(\omega) \sim \omega^s$, where the power $s \leq 1$ [14]. This and some other points, related to the *universal relaxation*, will be discussed in a later publication.

Results and discussion – demonstration of the methodology

In order to test and illustrate the power of the new EIS numerical analysis and the result shown in Fig. 4, three different condensed matter experimental systems have been chosen for further analysis and simulation. In

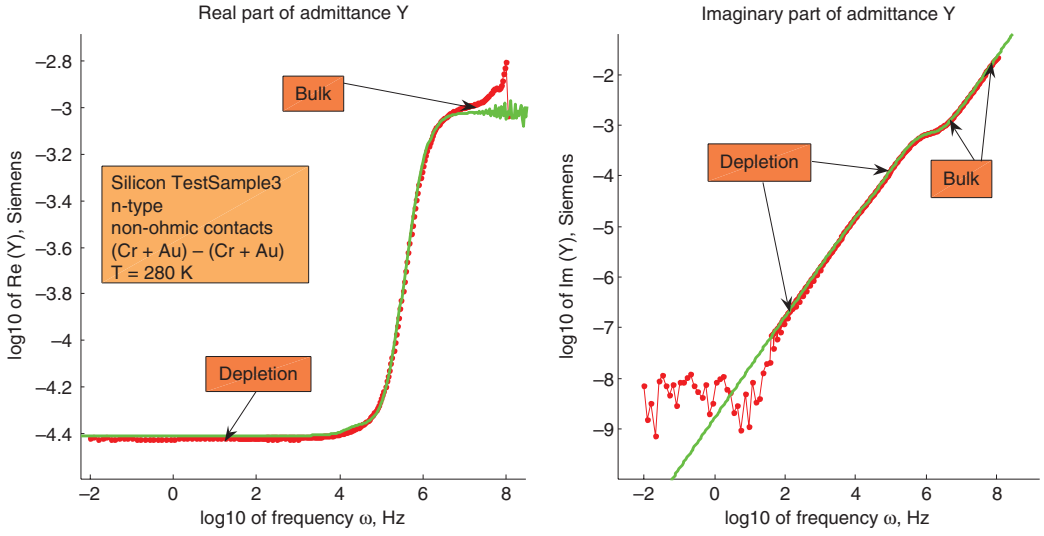

Fig. 4: Double logarithmic plot of the measured and calculated complex admittance $\tilde{Y}(\omega)$ as a function of frequency ω. Various parts of sample respond at various frequencies.

monocrystalline, ultra-pure Silicon, the temperature and the dc voltage bias dependence of the electrical impedance have been measured and analysed. The effect of the residual deep defect level within Silicon electron energy band gap on the overall electrical response has also been investigated. The second system chosen has been chalcogenide glass ion conductor $Ag_x(AsS_2)_{1-x}$. Here, the main focus has been the simultaneous determination of Ag^+ ion density and mobility. The third experimental system has been a simple aqueous NaCl solution, to illustrate, within the framework of the new EIS numerical analysis, the usefulness of the equivalent R, C, L networks, defined by the new EIS analysis, in modelling the electrical response in liquids.

Monocrystalline Silicon

Monocrystalline Silicon samples were small platelets (Area $\sim 1.0 \cdot 10^{-4}$ [M^{+2}], Thickness $\sim 0.5 \cdot 10^{-3}$ [M]), with various metal electrodes, evaporated on the corresponding optically flat and polished surfaces. The electrical contact were of Schottky-Schottky, Schottky-Ohmic and Ohmic-Ohmic type, through appropriate implantations and subsequent recrystallisation/annealing. The samples were prepared with various concentrations of either n or p type shallow dopants (P and B).

A typical temperature and dc voltage bias dependence of the measured and fitted electrical impedance in the chosen model semiconductor is shown in Figs. 5 and 6.

The effect of the residual defect deep level, shown in Fig. 3 in real time response, is best visualised when plotted as a real part of the complex capacitance $\tilde{C}(\omega)$ in the frequency domain. This is done in Fig. 7.

The agreement between the new EIS numerical analysis and the experiments, shown in Figs. 5–7, is very good indeed and it gave confidence when later studying less known systems such as non-crystalline materials, viscous liquids and other complex disordered systems.

The presented new approach to the analysis of EIS experiment has turned out to be quite powerful. It enables the determination of a large number of the electrical material parameters in the SUT. As an illustration, Table 1 shows the electrical material parameters that have been determined for the presented case of monocrystalline Silicon with a single deep level defect (Phosphorus-Vacancy defect complex [16, 17]).

The values of the various parameters in Table 1 that are in red, signify either that they have not been determined previously or that they differ somewhat from the literature/consensus values.

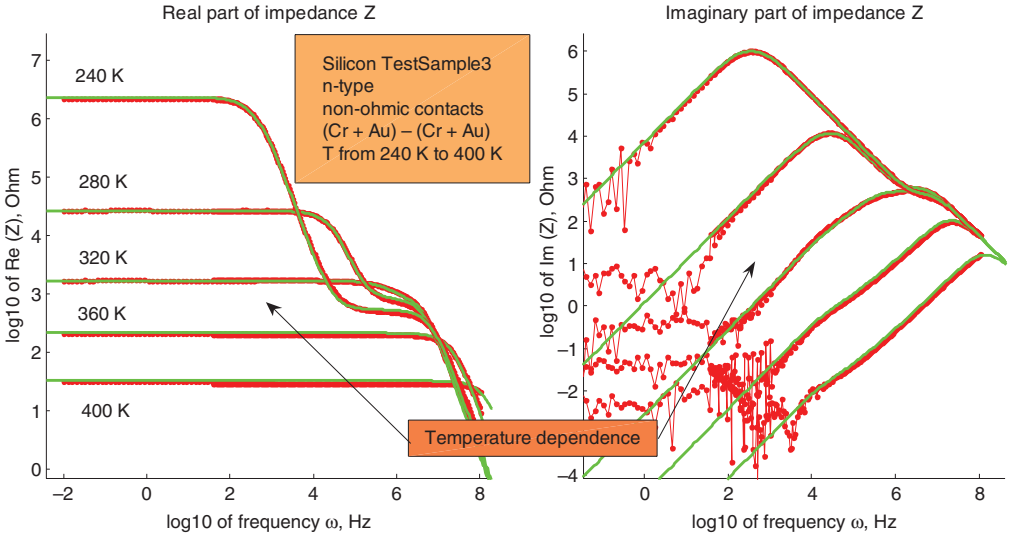

Fig. 5: Temperature dependence of the measured and calculated complex impedance $\tilde{Z}(\omega)$ as a function of frequency ω in Silicon TestSample3.

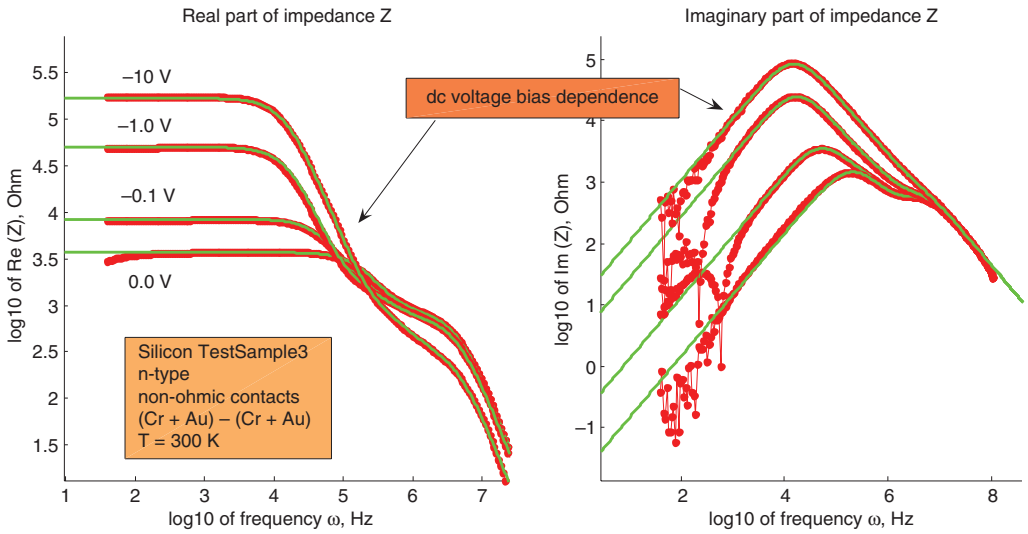

Fig. 6: dc voltage bias dependence of the measured and calculated complex impedance $\tilde{Z}(\omega)$ as a function of frequency ω in Silicon TestSample3.

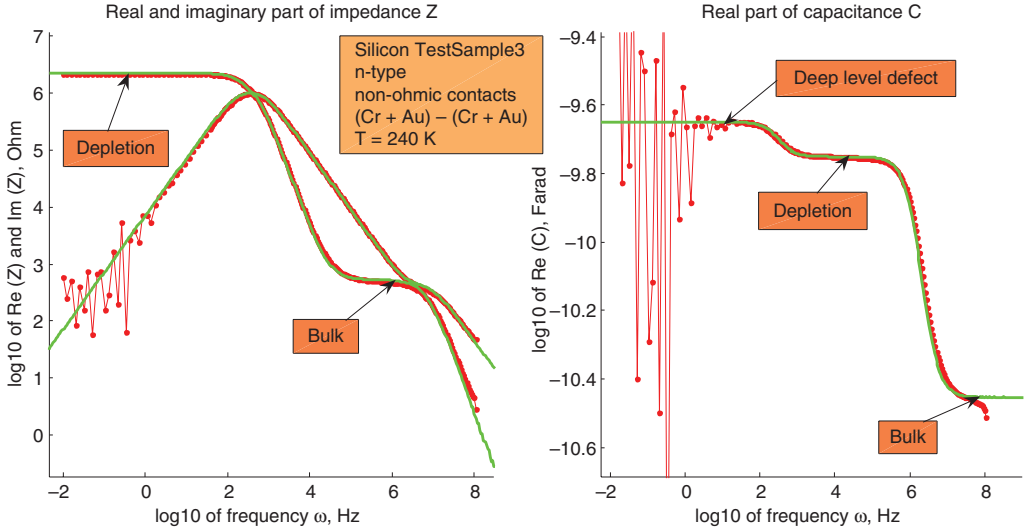

Fig. 7: Plot of complex impedance $\tilde{Z}(\omega)$ and of the real part of complex capacitance $C_1(\omega)$ as a function of frequency ω. The contribution to the response from a deep level clearly visible in the real part of the complex capacitance.

Approximate, equivalent R, C, L circuit modelling of the response

Another important result of the new EIS analysis is that the numerical analysis seems to define quite uniquely the appropriate R, C, L networks that can be used as analytic approximations to the full numerical analysis. The topology of the networks is related both to the possible spatial variations of the electrical material parameters of the SUT and to the number of independent physical processes contributing to the overall electrical response. In the first case (spatial variations), the network is divided into a number of characteristic impedances in series and in the second case (various physical processes active), each of these characteristic impedances is made of a number of characteristic admittances in parallel, each of these admittances describing the contribution to the electrical response from a particular physical process, such as fast polarisation, dc conduction, slow, possibly universal polarisation, deep level polarisation, *quasi*-ballistic trans-

Table 1: Values of various electrical material parameters in Silicon as determined by new EIS numerical analysis of electrical impedance measurements on a number of ultra-pure monocrystalline Silicon samples.

Comment	Parameter	Literature or consensus	EIS value
Quantum mechanical	Density of states	N_c	$(0.9–1.2)\cdot N_c$
	Density of states	N_v	$(0.9–1.2)\cdot N_v$
	Cond. band edge	E_c	$1.0\cdot E_c$
	Valence band edge	E_v	$1.0\cdot E_v$
	Energy band gap [15]	Ego	1.17 [eV]
	Band gap T-dependence [15]	α (EgT)	7.5–8.4
	Dielectric constant	ε	$1.0\cdot\varepsilon$
Transport	Electron density bulk	ne(n-type, 300 K)	$1.55\cdot10^{17}$ [M^{-3}]
	Hole density bulk	nh (p-type, 300 K)	$1.07\cdot10^{18}$ [M^{-3}]
	Electron mobility [15]	μe0	$1.0\cdot\mu$e0
	Hole mobility [15]	μh0	$1.0\cdot\mu$h0
	El.Mob.Temp.Exp. [15]	αe	2.15
	Hole.Mob.Temp.Exp. [15]	αh	2.80
Interface	elchpotSl (Cr + Au)		−4.690 [eV]
	elchpotSl (Ti)		−4.550 [eV]
Deep level	Ei		−4.540 [eV]
	Ni		$(0.7–1.2)\cdot10^{17}$ [M^{-3}]
	ccj [15]		$(4–6)\cdot10^{-18}$ [$M^3\cdot S^{-1}$]
	(electron capture from E_c to E_j)		
	cvj [15]		$(4–6)\cdot10^{-18}$ [$M^3\cdot S^{-1}$]
	(electron capture from E_v to E_j)		
	type		Acceptor
Derived	Schottky barrier height (Cr + Au)		0.64 [eV]
	Schottky barrier height (Ti)		0.50 [eV]
	Depletion width W_D		~10 microns
	Debye screening length L_D		~1.0 micron
	Bulk conductivity	>10 000 [Ω · cm]	35 000 [Ω · cm]

port, superconductivity, etc. Also, the various R, C, L elements within the networks describing the various aspects of the response, are very often uniquely defined. They are expressed as analytic functions of the electrical material parameters of the SUT [2]. Taking the numerical results of the new EIS analysis, shown in Figs. 3 and 7, the corresponding equivalent R, C network is shown in Fig. 8.

Here the R_B and C_B are the sample bulk dc resistance and geometrical capacitance. The left and the right electrode-sample interface regions are represented by the left and right depletion resistances R_{LD} and R_{RD} and the respective geometrical capacitances C_{LD} and C_{RD}. The resistances represent the dc transport (current i in eq. 6), while the capacitances represent the fast polarisation process (electric induction $\vec{D}$ in eq. 6). The third physical process taking place in the chosen sample of Silicon monocrystal is the slow dielectric relaxation due to the presence of the residual deep level defect (Figs. 3 and 7). Its effect on the overall electrical response is largest around the spatial point where the defect energy level E_j crosses the electrochemical potential (black dashed-dot and violet dashed curves in Fig. 2), which happens within the depletion regions. This

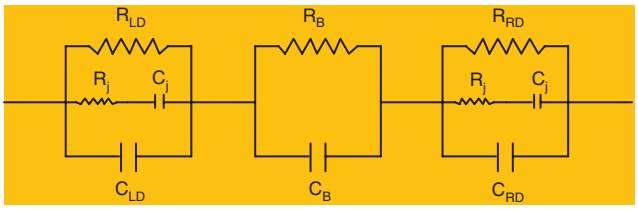

Fig. 8: The equivalent R, C electrical circuit network diagram, describing the electrical response of model semiconductor shown in Figs. 3 and 7.

slow polarisation process is represented by a series R_j, C_j terms in Fig. 8. The resistance R_j though is not the usual dc resistance, but it describes the characteristic relaxation time of the deep level relaxational process through relation $R_j = \tau_j / C_j$. The capacitance C_j is a measure of the strength of the relaxational polarisation. The R_j, C_j term models, what is known as Debye relaxation process. It will be argued later, that in order to model the relaxational behaviour of the deep level defect in the presented crystalline Silicon more precisely, the R_j, C_j term in Fig. 8 should be substituted by *universal capacitor* $\tilde{C}_{\text{univ}}(\omega)$. This type of capacitor models a very general class of slow dielectric relaxation phenomena, observed in many complex systems [11–13]. In the literature, it has been termed *Universal Relaxation* [12, 13] and in the frequency domain, it is usually of the form [18, 19]

$$\tilde{C}_{\text{univ}}(\omega) = \frac{C_0}{[1 + (i \cdot \omega\tau)^{1-\alpha}]^{1-\beta}}, \tag{16}$$

where C_0, τ, α and β are phenomenological, fitting parameters. When the terms R_j, C_j in Fig. 8 are substituted by $\tilde{C}_{\text{univ}}(\omega)$, the deep level response in Silicon, shown in Fig. 6, is captured quite precisely.

The analytic expressions for all of the R, C elements in Fig. 8 are given in the reference [2]. An extra note should be added at this point. The various R's and C's in Fig. 8 are not a complete description of the corresponding physical processes just discussed. In general, each R describing conduction process has an inductor in series, while each C, describing polarisation process has a resistor in series. These elements are omitted here, because they become active first at high frequencies towards and sometimes even beyond 1 THz. Also important and very useful in general, is the observation that the physical processes that are described by the R, C network in Fig. 8 can often be very identified already in the raw data, when these are represented as complex impedance $\tilde{Z}(\omega)$, together with the real part of the complex capacitance $C_1(\omega)$ as is done in Fig. 7.

Determination of mobile charge density and mobility

The new EIS numerical analysis has shown that for real samples with electrode-sample interfaces, the electrical response is determined to a large extent by these boundaries. Due to the difference in the chemical potentials of the bulk sample and of the electrode material (see Fig. 1), there will always be a finite charge transfer across the electrode-sample interface, facilitated by the mobile charges, even in the state of thermodynamic equilibrium. This is often considered as an unwanted complication and many efforts are usually made to avoid this problem by treating the interfaces in such a way that they become *ohmic*, that is to say, low resistive relative to the resistance of the sample. When the electrical transport is studied by EIS, these efforts are unnecessary. One reason is that in a majority of experimental situations, the response of the sample bulk and the response of the interface regions are well separated in frequency and can therefore be studied separately, bulk at higher frequencies and the interfaces at lower frequencies. However, there is an even more important reason, why one should aim at well defined, *non-ohmic* contacts. It is that the *non-ohmicity* of contacts that leads to non-zero charge transfer across the electrode-sample interface, affects the measured capacitance of the SUT (sample + electrodes) which is related directly to the electrical mobile charge density.

The principal possibility of independent and simultaneous determination of the mobile charge density and the mobility is considered as one of the most important results of the new EIS numerical analysis. To further illustrate this important point, Fig. 9 shows the effect of changes in the density and the mobility of mobile charges on the functional form of the real part of the complex capacitance in Silicon test sample.

As can be seen in Fig. 9, the changes in the values of density n_B and mobility $\mu(E_j)$, affect the real part of the complex capacitance $C_1(\omega)$ in a different way. The changes in mobility (violet curves) do not change the low frequency plateau in $C_1(\omega)$ which is uniquely related to the density of electrical mobile charges n_B.

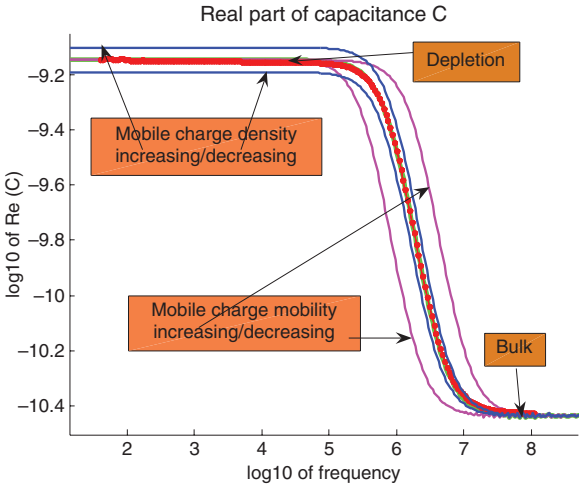

Fig. 9: Changes in the real part of the complex capacitance $C_1(\omega)$ in Silicon sample, caused by the changes in the density and the mobility of mobile charges.

Similarly, the changes in n_B (blue curves) do not affect in any significant manner the transition region from depletion to bulk capacitance.

Chalcogenide glass ion conductor $Ag_x(As,S_2)_{1-x}$

The presented new method how to determine independently, simultaneously and in one EIS experiment both the mobility and the mobile charge density has been applied to the case of chalcogenide glass ion conductor $Ag_x(AsS2)_{1-x}$. The samples were small platelets (Area $= 2.6 \cdot 10^{-5}$ [M^{+2}], Thickness $= 1.2 \cdot 10^{-3}$ [M]) with varying concentrations of Silver. The electrodes were sputtered Au films. The measurements and the new numerical EIS analysis fit results on the Ag rich sample are shown in Fig. 10.

The raw EIS data in Fig. 10 are more complicated than in the case of Silicon mono-crystal, mainly due to the presence of the slow universal relaxation within the thin metal electrode–sample interface region. The

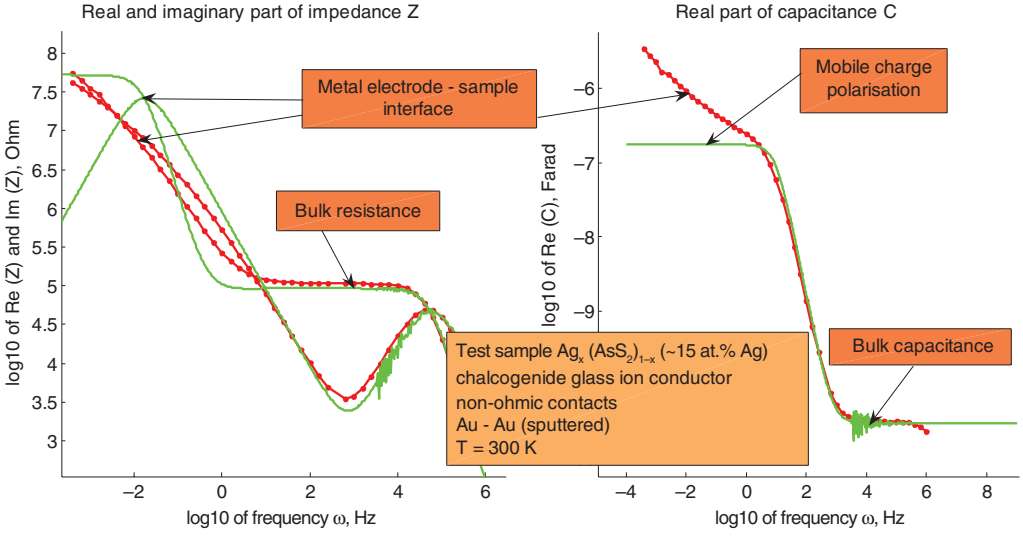

Fig. 10: The plot of the complex impedance $\tilde{Z}(\omega)$ and of the real part of the complex capacitance $C_1(\omega)$ in chalcogenide glass ion conductor $Ag_x(AsS2)_{1x}$ (~15 at.% of Ag) as a function of frequency ω. The red dots are experiment, the green curves are the new EIS numerical analysis best simulation fit results.

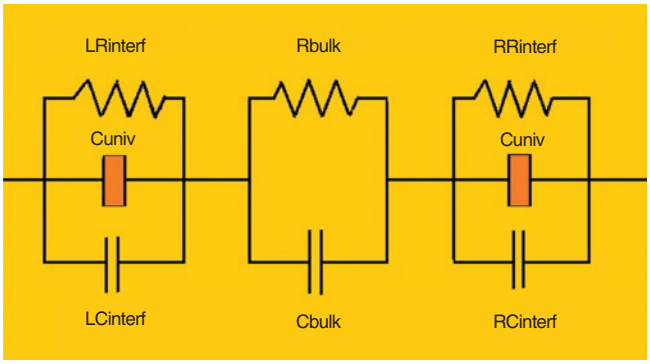

Fig. 11: The equivalent R, C electrical network circuit, describing the response of the Ag rich chalcogenide glass ion conductor $Ag_x(AsS2)_{1-x}$.

effect of this is a poor fit at low frequencies and a poorly resolved depletion capacitance, marked mobile charge polarisation in Fig. 10, where $C_1(\omega)$ does not level-off as $\omega \to 0$. Despite this complication, it has been possible to determine both the mobile charge density and the mobility:

- Density of the positive mobile charges: $7.5 \cdot 10^{23}$ [M^{-3}]
- Mobility of the positive mobile charges: $3.82 \cdot 10^{-9}$ [$M^2/V \cdot s$]

These results are in sharp conflict with the values of the Ag atom diffusion constant, determined by the radioactive trace method. This disagreement indicates that the two transport processes, the electrically active mobile charge transport, where Ag^+ ion or Ag^+ ion-defect complex move under the influence of both concentration gradient and the electrical field, and possibly electrically neutral Ag atomic diffusional transport, where Ag atom or Ag^+ ion move only under the influence of concentration gradient, might not be the same. At present therefore, it is felt that the question of the true nature of the electrically active species in $Ag_x(AsS2)_{1-x}$ glass ion conductor is still open. It might be worthwhile to mention in this context that similar controversy also exists in mono-crystalline Silicon, where below ~300 °C, the Phosphorus shallow dopant is almost totally immobile, while the Phosphorus-Vacancy defect complex is highly mobile and can anneal out already at ~300 °C [16, 17].

The somewhat unsatisfactory fit in Fig. 10 can be improved appreciably when one takes into account the time/frequency dependence of the slow polarisation process within the interface and uses the equivalent R, C electrical network circuit according to the results of the new EIS analysis. Substituting the terms R_j, C_j in Fig. 8 by the universal response term $\tilde{C}_{univ}(\omega)$, the equivalent R, C electrical network circuit of Fig. 8 becomes now one, shown in Fig. 11.

The agreement between the experiment and the new EIS analysis simulation result now improves appreciably, as can be seen in Fig. 12.

According to the best EIS numerical analysis fit, the slow universal relaxation originates first of all from within the interfaces and not from within the bulk of the glass. In the present case, shown in Fig. 10, the possible contribution of the universal relaxation from within the bulk is not measurable at all in the blue curve (~15 at.% Ag sample) and it is present only as a smaller contribution to the overall response in the green curve (~10^{-3} at.% Ag sample).

Aqueous sodium chloride solution

In this third illustrative test case, the main purpose of the study has been the determination of the absolute electrical mobility of various hydrated ions in simple aqueous chloride solutions, using EIS method. A typical result for aqueous 10^{-3} molar sodium chloride solution is presented here.

The electrochemical measurement cell was made of silica glass, equipped with fused circular Platinum electrodes. The area of Pt electrodes was ~$3.0 \cdot 10^{-4}$ [M^{+2}] and their separation ~$5.0 \cdot 10^{-3}$ [M].

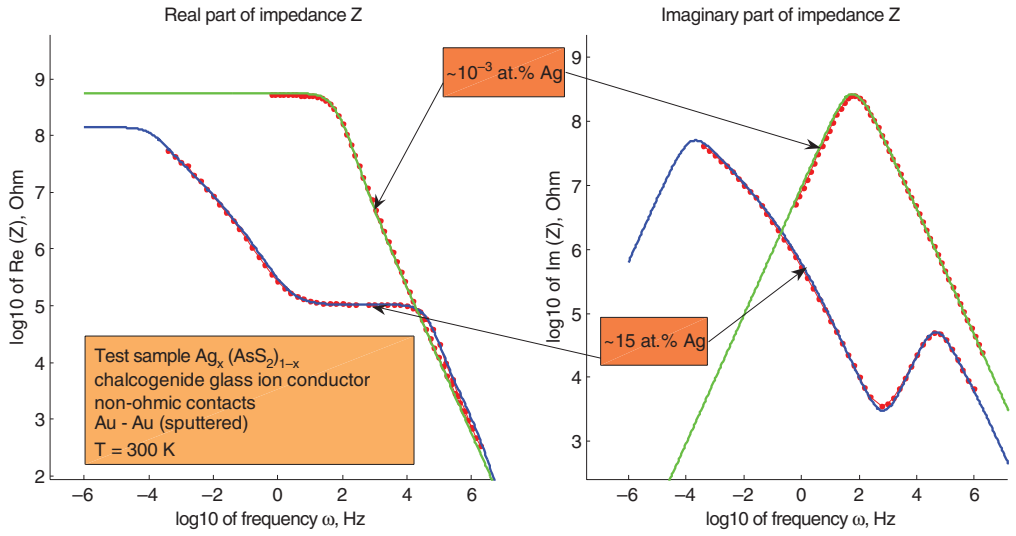

Fig. 12: The complex electrical impedance $\tilde{Z}(\omega)$ in $Ag_x(AsS_2)_{1-x}$ chalcogenide glass ion conductor as a function of frequency ω for two Ag concentrations. Universal relaxation included in the R, C model.

The new EIS numerical analysis and the approximate equivalent R, C electrical network circuit analysis has identified universal dielectric relaxation phenomenon also in this system. As has been the case with chalcogenide glass ion conductor, this response originates also in this case, from within the interface regions of SUT (Right Pt electrode – aqueous solution of NaCl-Left Pt electrode) as shown schematically in Fig. 11. The result of a typical EIS analysis for the 10^{-3} mol.% NaCl–H_2O solution is shown in Fig. 13.

The thickness of the determined interface region is smaller than in the case of chalcogenide glass Ag^+ ion conductor and is of the order of the distance between the Pt metal electrode-liquid interface and the first Helmholtz plane, at ~10 Å away into the solution.

The general behaviour of this liquid system with blocking electrodes (no ions pass through the Pt metal electrode-NaCl solution interface, neither are they deposited on the respective Pt metal electrodes' surfaces)

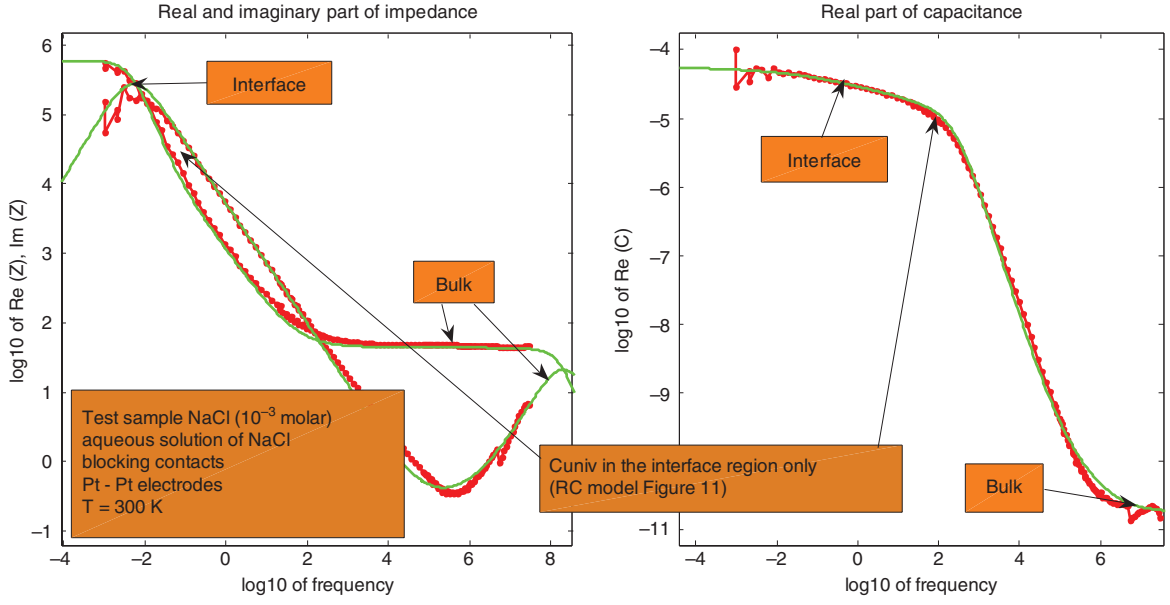

Fig. 13: Plot of the complex impedance $\tilde{Z}(\omega)$ and of the real part of complex capacitance $C_1(\omega)$ as a function of frequency ω in aqueous solution of NaCl (10^{-3} molar), measured at 300 K. Universal Relaxation included in the R, C model.

can be described as a combination of two processes. The first process is the drift-diffusion transport within the bulk of the NaCl solution. The second process is the redox reactions controlled local densities of ionised and neutral Na and Cl atoms within the respective thin interface regions.

The drift-diffusion flow of ions from the bulk region of the solution towards the respective electrodes and the effective electron transfer and the pure diffusional out-flow of electrically neutral Na and Cl atoms from the respective interface regions towards the bulk region of the solution (inclusive their eventual space dependent re-ionisation) then secures the necessary steady state, as observed experimentally. The steady state can be inferred from the constancy of the low frequency real part of the measured complex impedance (~$5.6 \cdot 10^5$ Ohm at ~10^{-4} Hz, see Figure 13 above) and from the constancy of the bulk solution resistance (plateau in the real part of the measured complex impedance between 10^4 and 10^8 Hz, see Figure 13 above).

The above presented example illustrates the power of the new EIS numerical analysis and simulations also within the field of Electrochemistry. The incorporation of the interfaces as essential part of the numerical analysis of EIS experiment, offers here a unique possibility to properly analyse the microscopic nature of redox reactions not only in this relatively simple system, but also in more complex systems, such as batteries, involving more complicated forms of interface electrochemical reactions.

EIS and other electrical characterisation methods

It has been argued throughout the present article, that the new numerical analysis of the electrical impedance measurements has placed Electrical Impedance Spectroscopy method on a new qualitative level, despite its present practical limitations, such as the neglect of magnetic fields and of time independence of the dielectric permittivity in the full numerical analysis. The electrical material parameters of SUT that new EIS analysis enables to be determined, could only be determined previously by a combination of a number of existing experimental methods.

When analysing these other methods, it has turned out that many of them are in fact just either a single point on or a part of the measured EIS impedance curves. To illustrate this point, the main results of the new EIS numerical analysis, shown in Fig. 3 (time domain response) and Fig. 7 (frequency domain response) are re-plotted below in Fig. 14, with other methods placed on the respective EIS response curves.

Two experimental methods have been chosen to illustrate the usefulness and the applicability of the new EIS numerical analysis and electrical response simulations in the real time domain. At short times, it is the Time Resolved Terahertz Spectroscopy (TRTS) experimental method, where the energy-space-time dynamics

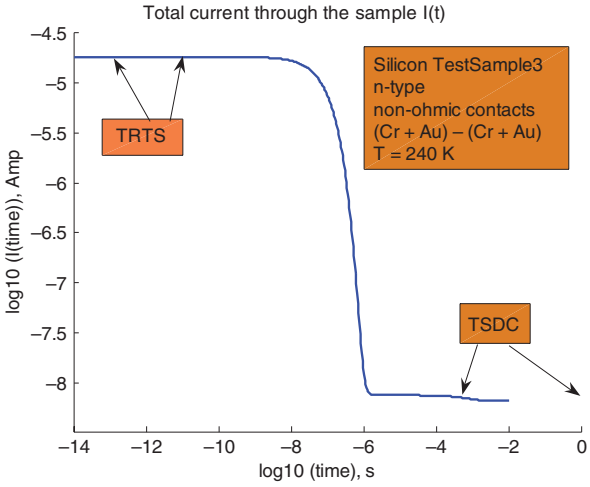

Fig. 14: Total electrical current $I(t)$ through the model semiconductor sample as a function of time after application of a step voltage. The two real time experimental methods (TRTS and TSDC) indicated.

of the electrical charges have to be modelled in more or less the same way as in EIS, regardless whether excess mobile charge carriers are generated by a laser pulse or not. The long times example is the Temperature Stimulated Depolarisation Current (TSDC) method, which is, in its simplified form, the measurement of the current response to polarisation voltage step input. It is, in fact, the real time extension of the frequency dependent EIS measurements down to frequencies where the single frequency measurement time becomes too impractical (in excess of 1 month).

While the techniques such as TRTS and TSDC do span some time intervals of the new EIS method in time domain, the other techniques, such as 4PDCR, I-V, C-V and DLTS, can be viewed just a single points on the EIS electrical impedance curves. This is illustrated in Fig. 15.

In regards the fundamental electrical material parameters that can be extracted from various electrical experimental techniques, Table 2 presents a summary for EIS and for some of these other experimental methods [20].

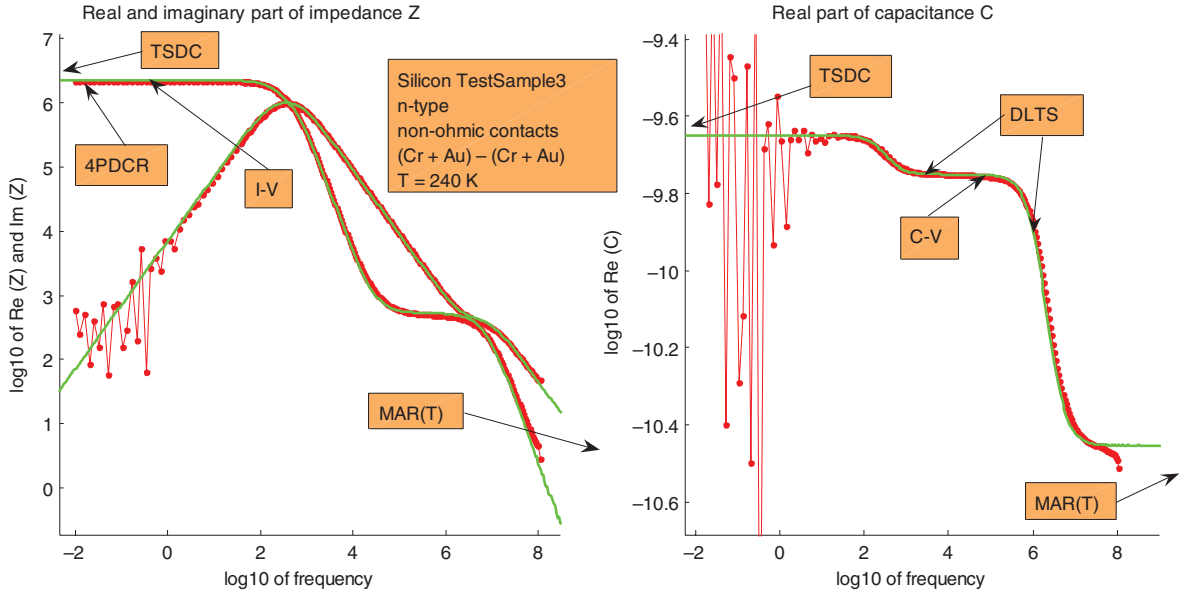

Fig. 15: Plot of complex impedance $\tilde{Z}(\omega)$ and of the real part of complex capacitance $C_1(\omega)$ as a function of frequency ω. Some of the other experimental methods indicated as single points on the EIS curves.

Table 2: Various experimental techniques and the electrical material parameters they can determine.

Exp. method	Parameter						
	$\tilde{\varepsilon}(\omega)$	μ	n	$\Delta\mu^{elchpot}$	ρ or σ	τ	DL
4PDCR					Yes		
HE		Yes	Yes				
FTIPL			Yes				
TOF		Yes					
CP				Yes			
PEE				Yes			
MAR(T)	Yes					Yes	
DRS	Yes						
C-V			Yes				
I-V					Yes		
DLTS							Yes
TSDC	Yes						
TRTS	Yes						
New EIS	Yes	Yes	Yes	Yes	Yes	Yes	Yes

Table 3: Various experimental techniques and the necessary conditions and limitations for a given parameter determination.

Abbreviation	Measuring method	Quantity measured	Condition/comment
4PDCR	Four probe dc resistance [20]	ρ [$\Omega \cdot M$]	Standard and van der Pauw higher conductivity materials
HE	Hall effect [20]	n [M^{-3}], μ [$M^2 \cdot V^{-1} \cdot S^{-1}$]	Magnetic fields required Valid only for crystals
FTIPL	Fourier transform infrared photo-luminescence [2, 20]	n [M^{-3}]	Helium temperatures required, indirect
TOF	Time of flight [20]	μ [$M^2 \cdot V^{-1} \cdot S^{-1}$]	
CP	Contact potential [2]	$\Delta\mu^{elchpot}$ [eV]	
PEE	Photo electron emission	$\Delta\mu^{elchpot}$ [eV]	Ultra-High Vacuum required
MAR(T)	Microwave absorption reflection (transmission)	$\tilde{\varepsilon}(\omega)$ [$F \cdot M^{-1}$]; τ [S]	Is contactless
DRS	Dielectric relaxation spectroscopy	$\tilde{\varepsilon}(\omega)$ [$F \cdot M^{-1}$]	Variant of EIS
C–V	Capacitance–voltage measurements [20]	n [M^{-3}]	Usable only on well-defined Schottky barriers
I–V	Current–voltage measurements	ρ [$\Omega \cdot M$]	
DLTS	Deep level transient spectroscopy [20]	DL	Only partial characterisation
TSDC	Thermally stimulated depolarisation currents	$\tilde{\varepsilon}(\omega)$	Long, real time measurements; extension of EIS towards dc
TRTS	Time resolved tetrahertz spectroscopy	$\tilde{\varepsilon}(\omega)$	Ultra short laser pulse needed Is contactless
New EIS	Electrical impedance spectroscopy	All parameters in Tables 1 and 2	EIS with new numerical analysis Simple, precise and very general

Parameter symbols in Table 2 are dielectric permittivity $\tilde{\varepsilon}(\omega)$, electrical mobility μ, the density of the mobile charges n, the difference in the electrochemical potential across the interface metal electrode-sample $\Delta\mu^{elchpot}$, dc resistivity ρ or dc conductivity σ, the life time of excess mobile charges τ and deep level characteristics (see Table 1) DL.

Finally, the abbreviations for the specific experimental methods, together with some comments, relevant to Table 2, are presented and explained in Table 3.

Conclusions

A new approach to Electrical Impedance Spectroscopy numerical analysis has been presented. It is based on following energy and space-time evolution of the total, local electrical charge density $\rho(x, t)$ as a response of the material to a voltage step perturbation. The Laplace transform of the real time admittance gave then the experimentally measurable complex electrical admittance $\tilde{Y}(\omega)$ of the System under Test.

The new EIS numerical analysis has proved to be very powerful and has placed the EIS experimental method on a new qualitative and quantitative level, enabling, among other things:

- complete electrical characterisation of various materials
- experimental determination of the whole range of electrical material parameters in studied materials
- simultaneous determination of mobile charge density and mobility
- detailed studies of the electrical properties of interfaces
- real time simulations and modelling of charge dynamics
- modelling of the electrical response by an approximate equivalent R, C, L circuit network(s) with proper topology, where in most cases, the values of the R, C, L elements are analytic functions of the studied electrical material parameters [2].

The wide applicability of the new EIS method within the Condensed Matter Physics has been demonstrated on three, quite different experimental systems, monocrystalline Silicon, Chalcogenide glass ion conductor and aqueous Sodium Chloride solution.

It is now also argued, that based on the new numerical EIS analysis, the EIS experimental method has become the proper extension of optical spectroscopies from THz to dc.

At present stage, there are some remaining issues to be resolved in order to complete the EIS numerical analysis. The two most important are the inclusion of magnetic field into the governing set of equations and the second is relaxing the requirement of the time independence of the electrical permittivity (slow dielectric relaxation processes inclusive the universal relaxation) and mobility (quasi-ballistic transport). The work along these lines is in progress.

Acknowledgements: The authors would like to thank professor Tomáš Wágner for kindly supplying chalcogenide glass ion conductor samples and Dr. Vítězslav Zíma for performing and making available, for further analysis, the EIS measurements on this glass system. One of the authors (PV) thanks the head of the Institute of Applied Physics and Mathematics, University of Pardubice, professor Čestmír Drašar, for welcoming him to the Institute. At the same time, he would like to express his sincere appreciation for stimulating discussions with Čestmír Drašar, Max Fraenkl, Tomáš Plecháček, Vít Zajac, Petr Zajíček and Vítězslav Zíma.

References

[1] M. A. Ozarem, B. Tribollet. *Electrochemical Impedance Spectroscopy*, 2nd edition, John Wiley, Hoboken, NJ, USA (2017).
[2] P. Viščor, J. Vedde. Method and Apparatus for determining characteristic electrical material parameters in semi-conducting materials. United States patent n. 5 627 479, May 6 (1997). European patent n. EP 067 2257 A1, September 20 (1995).
[3] E. Barsoukov, J. R. McDonald (Eds.). *Impedance Spectroscopy*, John Wiley, Hoboken, NJ, USA (2005).
[4] N. F. Mott, E. A. Davis. *Electronic Processes in Non-Crystalline Materials*, Clarendon Press, Oxford, UK (1979).
[5] P. Viščor. *Phys. Rev. B* **28**, 927 (1983).
[6] R. Balian, R. Maynard, G. Toulouse (Eds.). *Ill-Condensed Matter*, World Scientific, Singapore (1983).
[7] L. D. Landau, E. M. Lifshitz. *Statistical Physics I*, Pergamon Press, Oxford, UK (1980).
[8] L. D. Landau, E. M. Lifshitz. *Electrodynamics of Continuous Media*, Pergamon Press, Oxford, UK (1982).
[9] Ch. Kittel, H. Kroemer. *Thermal Physics*, W. H. Freeman and Comp., Stuttgart, Germany (1980).
[10] J. D. Jackson. *Classical Electrodynamics*, John Wiley, Hoboken, NJ, USA (1999).
[11] K. L. Ngai. *Relaxation and Diffusion in Complex Materials*, Springer-Verlag, Berlin, Germany (2011).
[12] A. K. Jonscher. *Dielectric Relaxation in Solids*, Chelsea Dielectrics Press Ltd., London, UK (1983).
[13] A. K. Jonscher. *Universal Relaxation Law*, Chelsea Dielectrics Press Ltd., London, UK (1996).
[14] M. Pollak, T. H. Geballe. *Phys. Rev.* **122**, 1742 (1960).
[15] R. Hull (Ed.). *Properties of Crystalline Silicon*, INSEC, London, UK (1999).
[16] P. Viščor, O. Andersen, T. Clausen, P. A. Ellsmore, L. Jensen. *ECS Trans.* **16**, 331 (2008).
[17] P. Viščor, O. Andersen, T. Clausen, P. A. Ellsmore, L. Jensen. *ECS Trans.* **16**, 109 (2008).
[18] S. Havrilliak, S. Negami. *Polymer* **8**, 161 (1967).
[19] S. Havriliak Jr., S. J. Havriliak. *Polymer* **37**, 4107 (1996).
[20] D. T. Schroder. *Semiconductor Material Device Characterisation*, John Wiley, Hoboken, NJ, USA (1998).